In Situ Surface Reconstruction of a Ni-based Perovskite Hydroxide Catalyst for an Efficient Oxygen Evolution Reaction

Yegui Fang[a], Yusheng Fang[a], Ruoqi Zong[a], Zhouyang Yu[a], Youkun Tao[b], Jing Shao[a*]

[a] College of Chemistry and Environmental Engineering, Shenzhen University, Shenzhen 518060, China;

[b]School of Science, Harbin Institute of Technology, Shenzhen 518055, China.

*Corresponding author

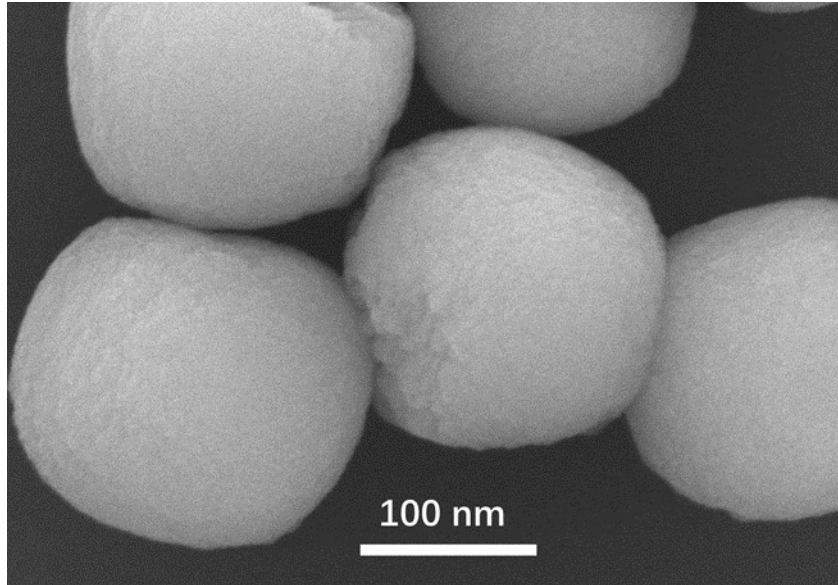E-mail address: shaojing@szu.edu.cn

Figure S1. SEM image of NiSn(OH)$_6$ nano particles prepared by coprecipitation method.
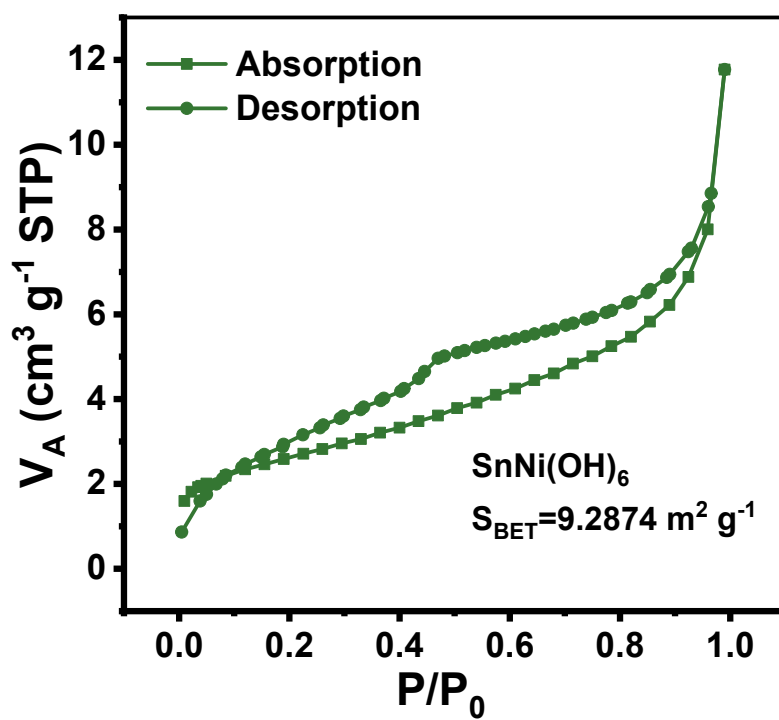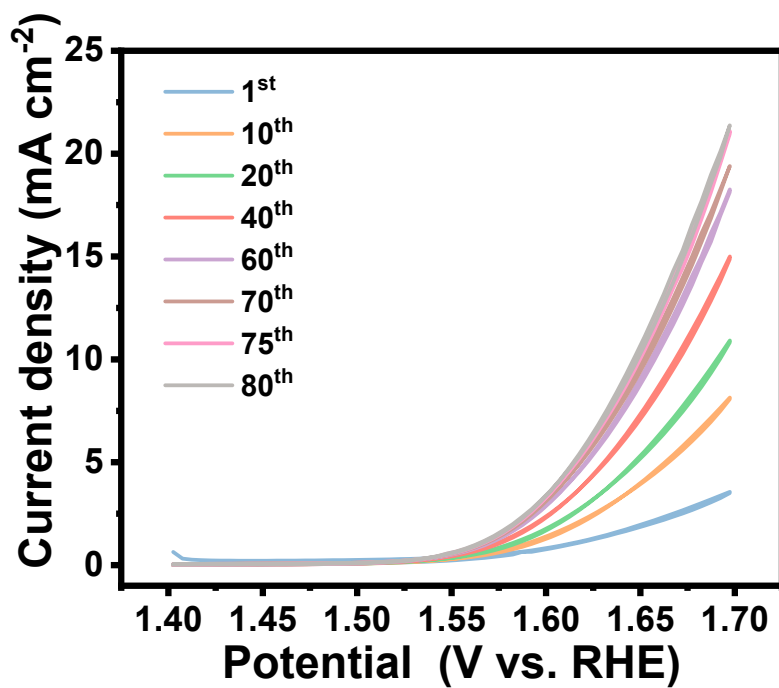
Figure S2. BET adsorption desorption curve of NiSn(OH)$_6$.

Figure S3. CV cycling curves on NiSn(OH)$_6$ in the potential range of 0.5 V-0.8 V (vs.

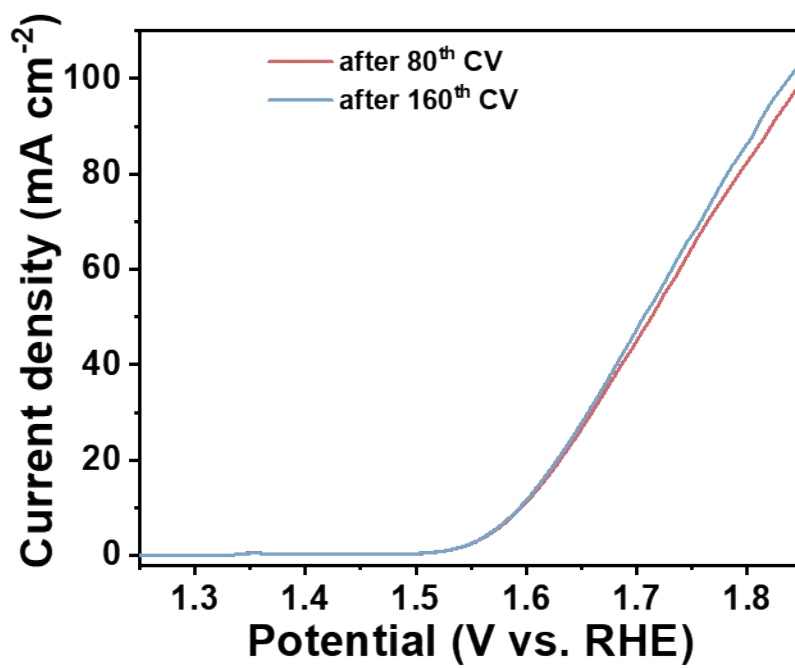Hg/HgO) with the sweep rate of 10 mV s^{-1}.

Figure S4. LSV curves of the catalyst after 80 CV cycles and after 160 CV cycles without iR correction.
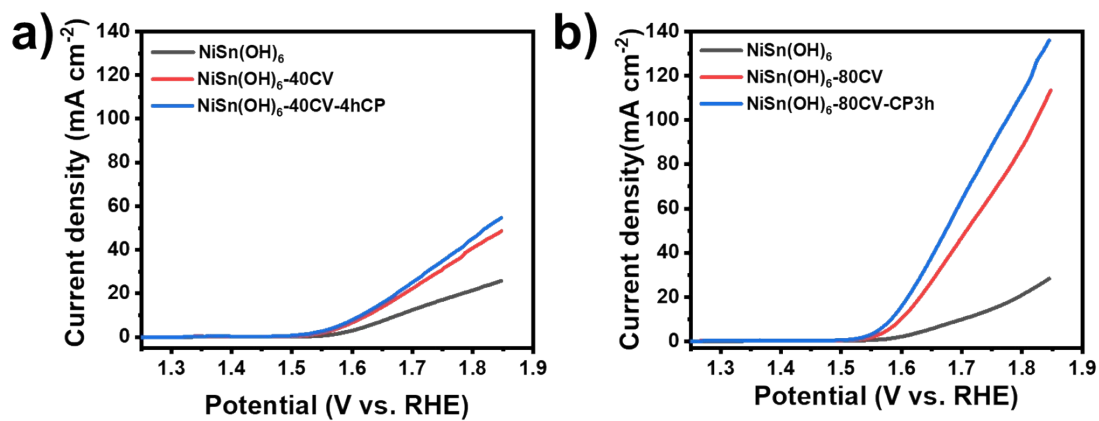
Figure S5. NiSn(OH)$_6$ activated by different procedures: (a) 40 CV cycles followed by galvanostatic polarization for 4 h; (b) 80 CV cycles followed by galvanostatic polarization for 3 h.
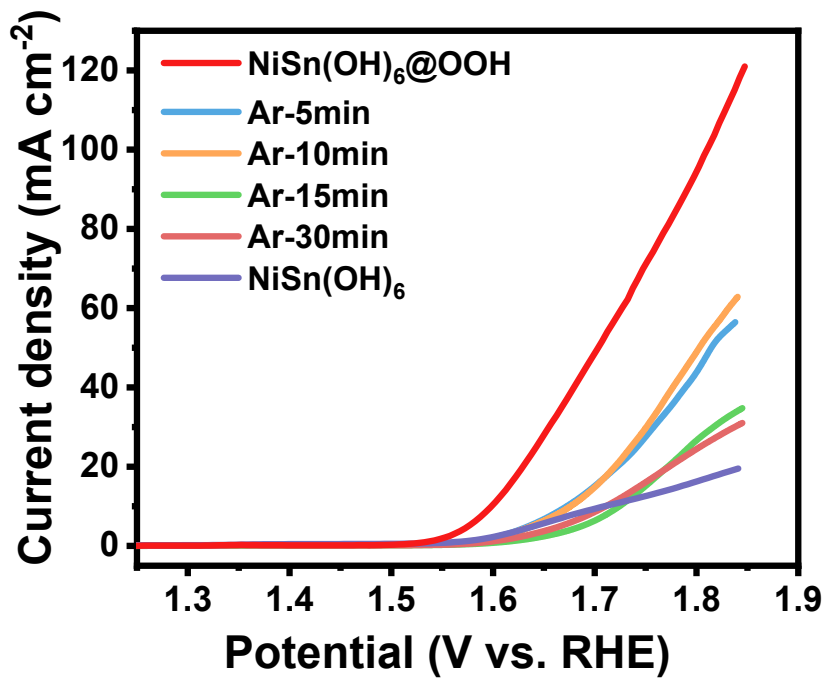
Figure S6. LSV curves without iR correction on NiSn(OH)$_6$ activated by CV cycling

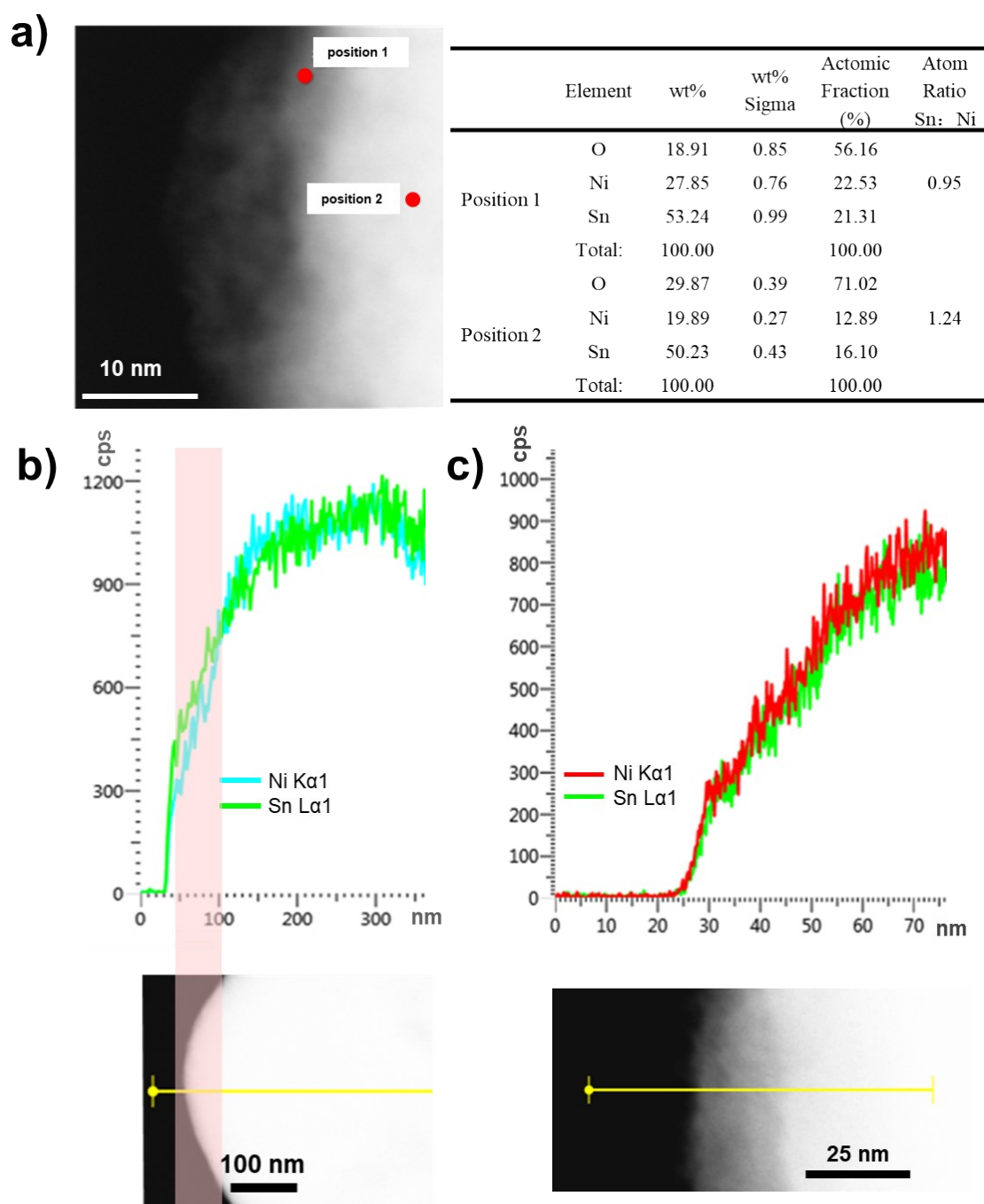(denoted as NiSn(OH)$_6$@OOH) and Ar plasma etching for different times.

a)

	Element	wt%	wt% Sigma	Actomic Fraction (%)	Atom Ratio Sn：Ni
	O	18.91	0.85	56.16	
Position 1	Ni	27.85	0.76	22.53	0.95
	Sn	53.24	0.99	21.31	
	Total:	100.00		100.00	
	O	29.87	0.39	71.02	
Position 2	Ni	19.89	0.27	12.89	1.24
	Sn	50.23	0.43	16.10	
	Total:	100.00		100.00	

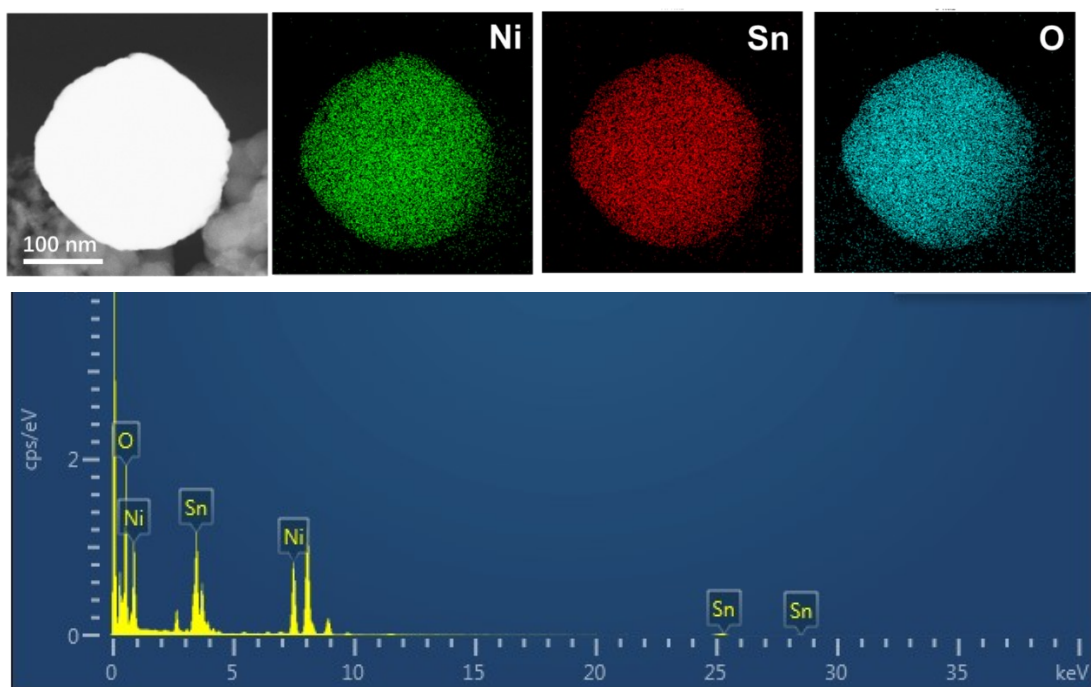**Figure S7.** (a) NiSn(OH)$_6$@OOH point scan and corresponding analysis, (b) NiSn(OH)$_6$ line scan path and corresponding analysis, (c) NiSn(OH)$_6$@OOH line scan path and corresponding analysis.
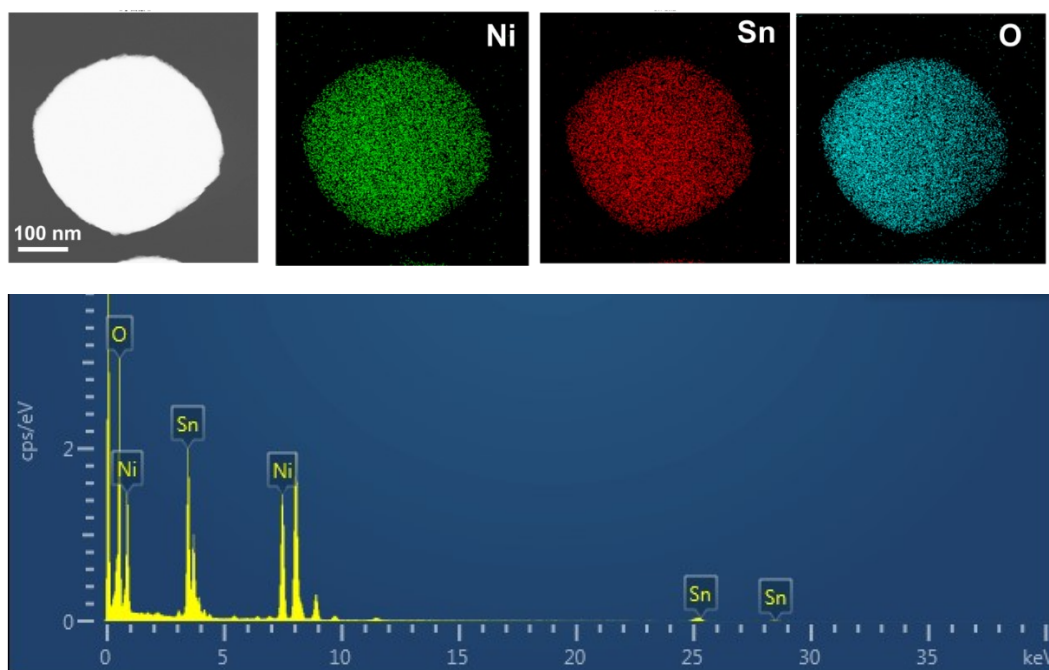
Element	Family	wt%	wt% Sigma	Atomic Fraction (%)
O	K	22.95	0.31	63.10
Ni	K	22.00	0.25	16.49
Sn	L	55.05	0.35	20.41
Total		100.00		100.00

Figure S8. EDS element mapping images of $NiSn(OH)_6$ and analysis.

Element	Family	wt%	wt% Sigma	Atom Fraction (%)
O	K	26.17	0.31	66.50
Ni	K	23.47	0.24	16.25
Sn	L	50.36	0.36	17.25
Total		100.00		100.00

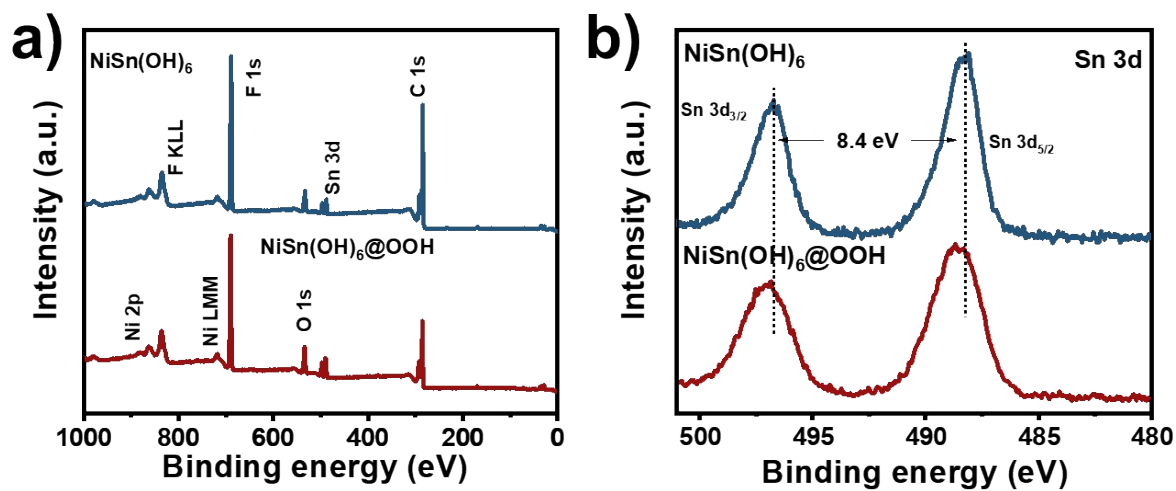**Figure S9.** EDS element mapping images of NiSn(OH)$_6$@OOH and analysis.

Figure S10. (a) XPS spectra of NiSn(OH)$_6$ and NiSn(OH)$_6$@OOH, (b) high-resolution
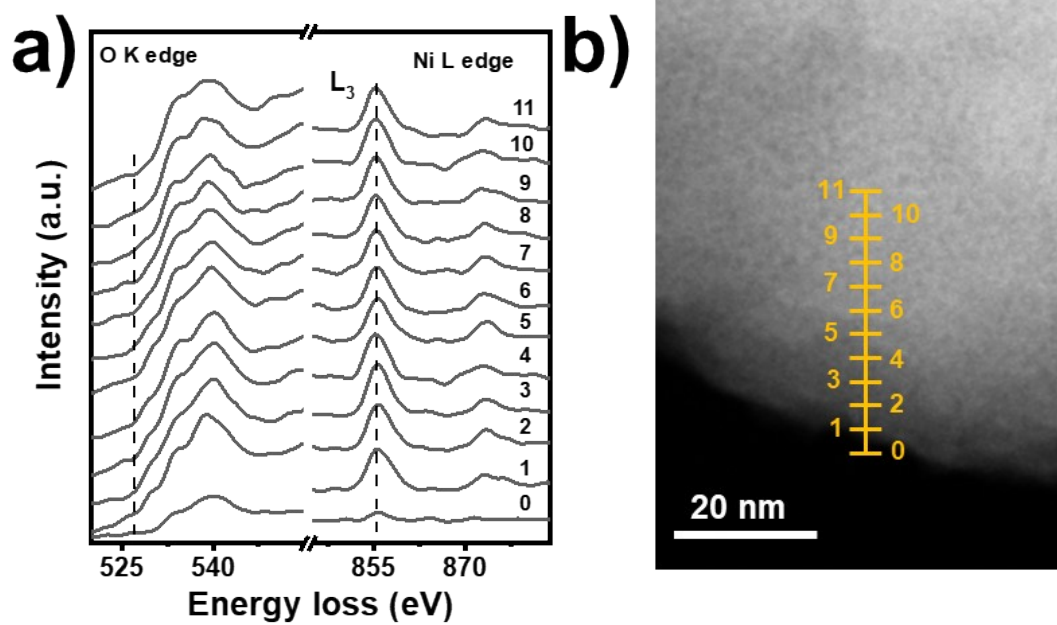
XPS spectra of Sn 3d.

Figure S11. The O K-edge and Ni L-edge EELS spectra collected along the junction to the outermost surface of NiSn(OH)$_6$. (b) STEM image of the corresponding scanning pathway for (a).
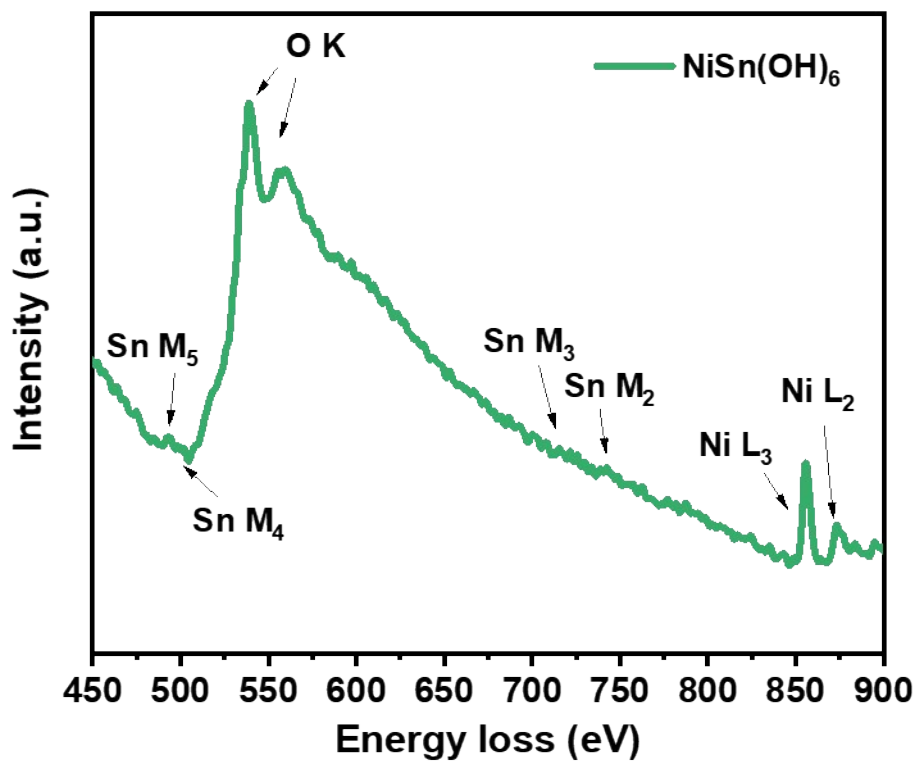
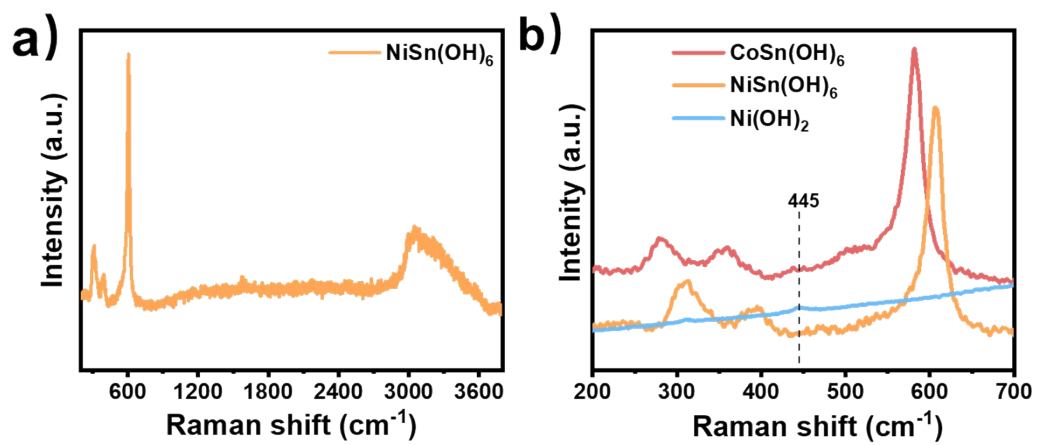**Figure S12.** The EELS spectra of Sn M-edge recorded on NiSn(OH)$_6$.

Figure S13. Raman spectra of $NiSn(OH)_6$, $CoSn(OH)_6$, and $Ni(OH)_2$.
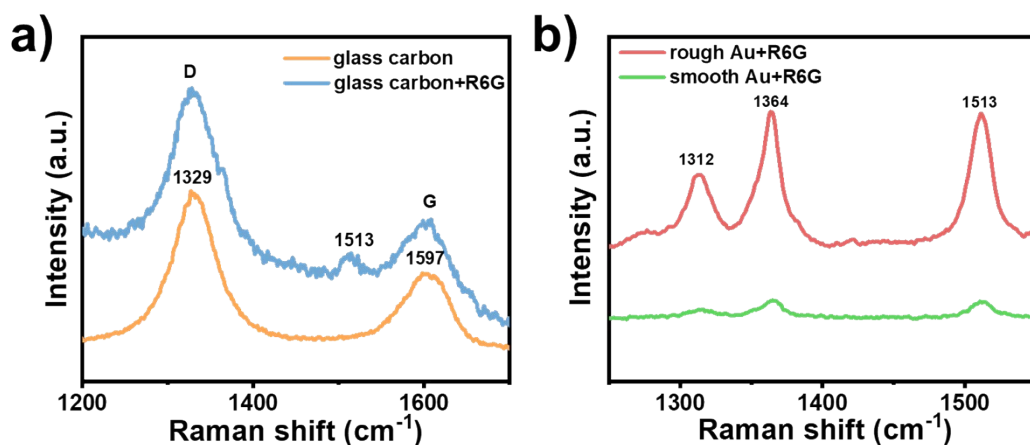
Figure S14. Raman spectra of R6G added on (a) glassy carbon electrode and (b) Au electrode with and without surface roughening. 10^{-3} mol L^{-1} of Rhodamine 6G (R6G) solution was dropped on different substrates, tested by Raman spectroscopy with excitation wavelength of 532 nm^{-1} and power of 10%.

The peaks at about 1329 cm^{-1} and 1597 cm^{-1} correspond to the disordered carbon atoms and sp^2-hybridized graphitic carbon atoms, which are the so called D band and G band.[1] The peaks at 1312 cm^{-1}, 1364 cm^{-1} and 1513 cm^{-1} are characteristic peaks of R6G.[2] The RS spetra of glassy carbon electrode dominated by the D band and G band with minor rhodamine signal. A weak R6G signal was observed for the untreated smooth gold sheet and a strong R6G signal was observed for the roughened gold substrate, indicating a significant SERS enhancement of the roughened gold substrate used in this paper, which can effectively improve the sensitivity of RS characterization for tracking the surface evolution of catalyst during the OER process.

1   Y. Wang, D. C. Alsmeyer and R. L. McCreery, Chem. Mater, 1990, 2, 557-563.

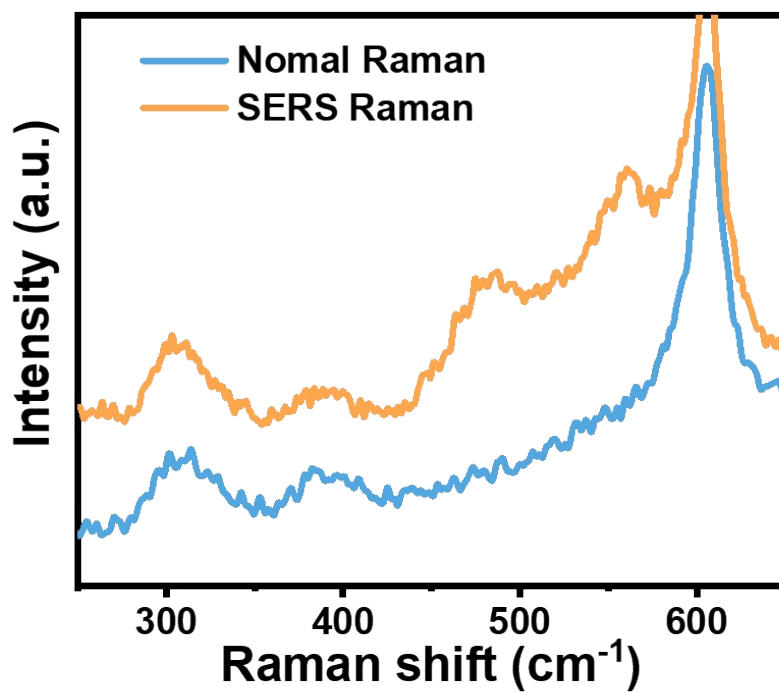2   Y. Liu, J. Lu, Y. Tao, N. Li, M. Yang and J. Shao, Anal. Chem., 2020, 92, 9566-9573.

Figure S15. Comparison of RS and SERS spectra of the $NiSn(OH)_6@OOH$ collected at
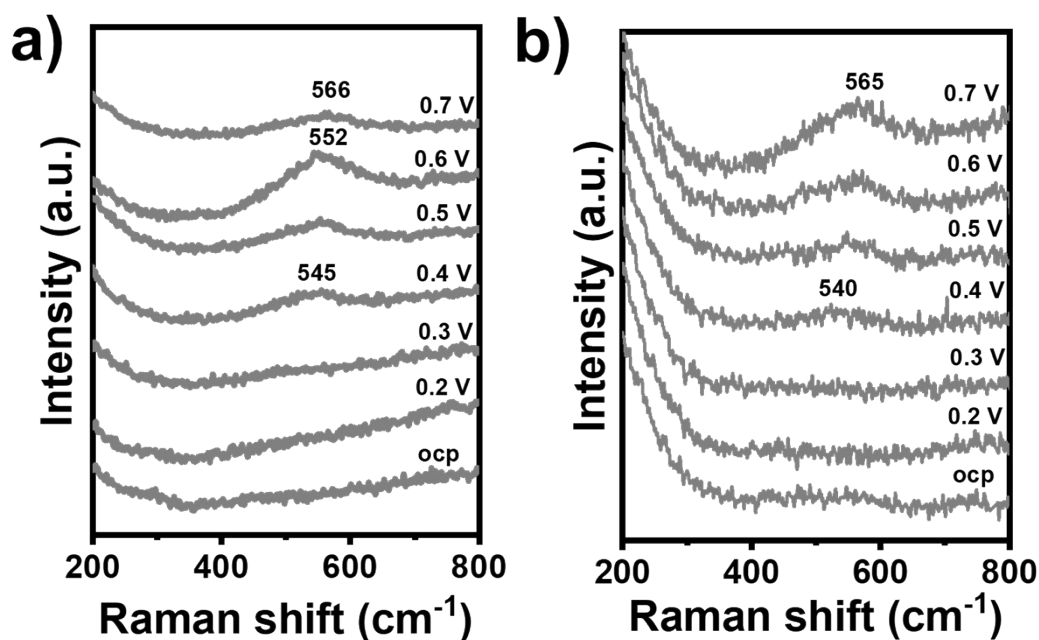
0.8 V (vs. Hg/HgO).

Figure S16. In situ RS analysis of the blank roughed gold substrate in 1 M KOH (a)

before and (b) after the CV cycling.

In order to clarify the possible effects of the polarization and CV cycling on the

SERS substrate, RS data was recorded on the blank roughed gold substrate during the

polarization process before and after the CV cycling. A broad peak appeared at 540-565

cm^{-1} above 0.3 V under both conditions. This peak was found to shift toward high wave

number with increasing the applied potential, which behavior is consistent with that

reported for the Au-O vibration in $Au(OH)_3$ in the literature.[1]

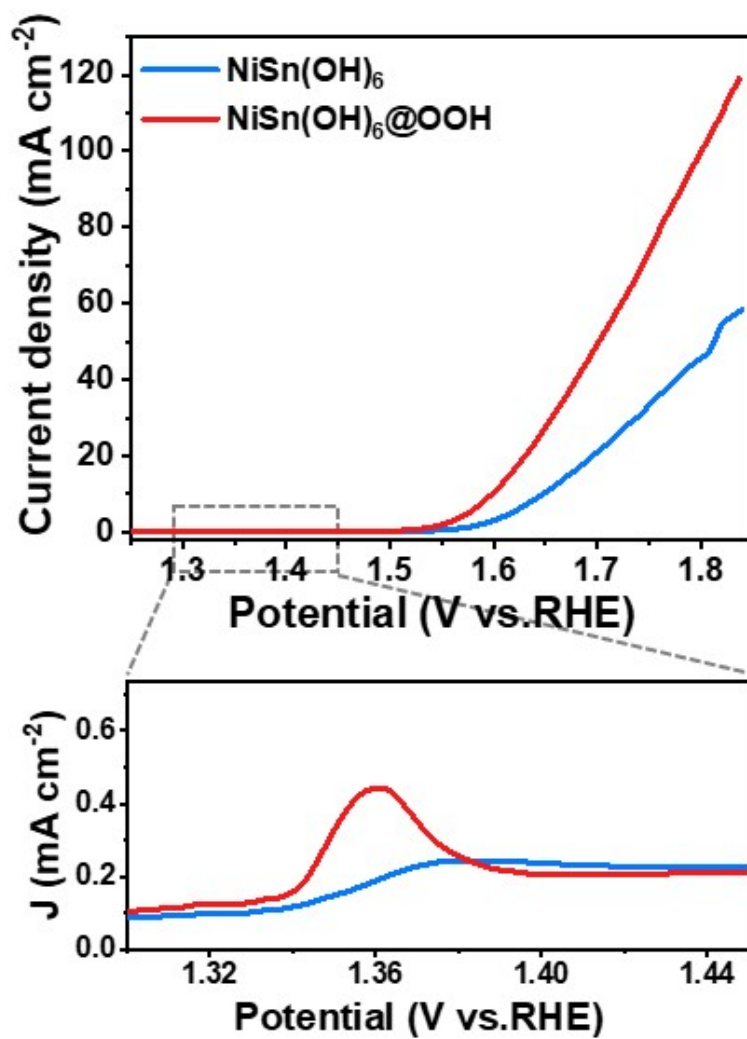1   M. W. Louie and A. T. Bell, J. Am. Chem. Soc., 2013,135, 12329-12337.

Figure S17. LSV curves without iR correction of the catalyst before and after the
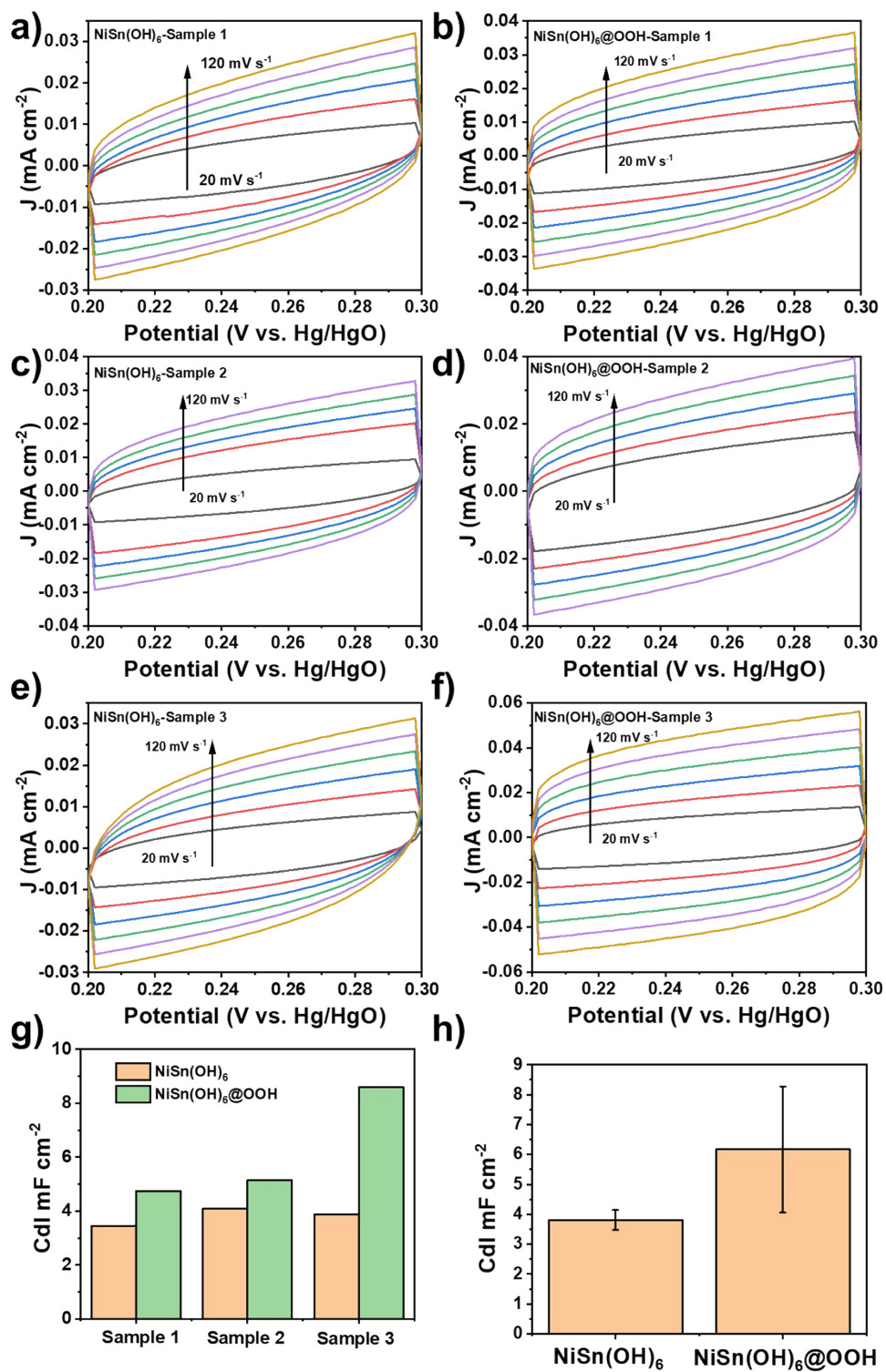
surface reconstruction process.

Figure S18. Double-layer capacitance measurements on NiSn(OH)$_6$ (a, c, and e) and

NiSn(OH)$_6$@OOH (b, d, and f): CV scan rates from 20mV s^{-1} to 120 mV s^{-1}; (g) and (h)

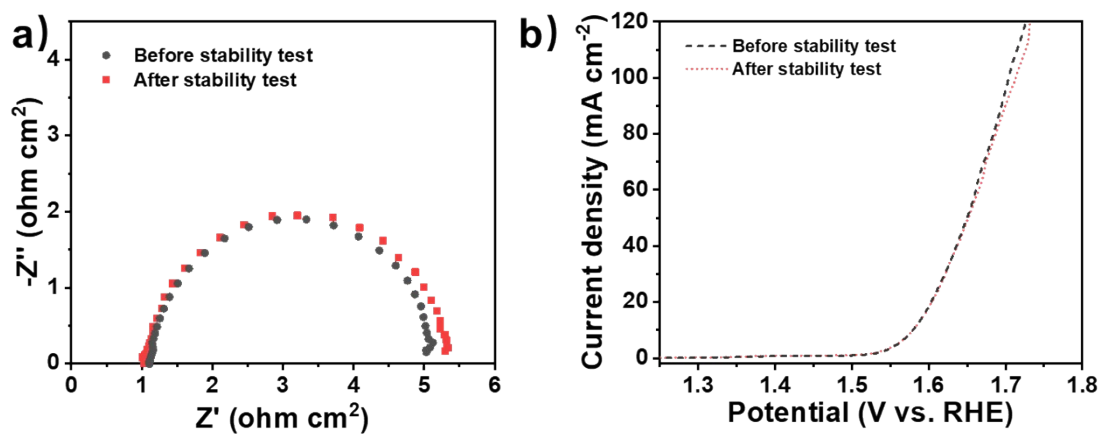calculated ECSAs of NiSn(OH)$_6$ and NiSn(OH)$_6$@OOH.

Figure S19. (a) EIS and (b) LSV curves of NiSn(OH)$_6$@OOH before and after stability
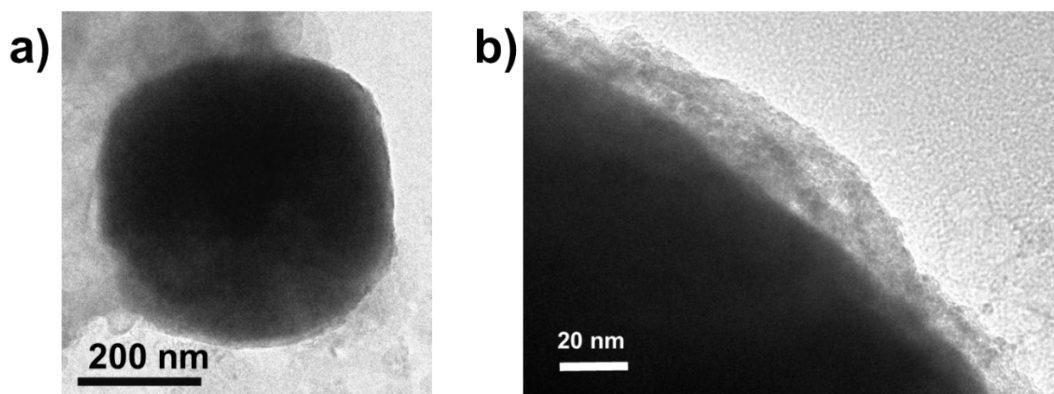
test.

Figure S20. (a) TEM and (b) HRTEM images of NiSn(OH)$_6$@OOH after 40,000 s
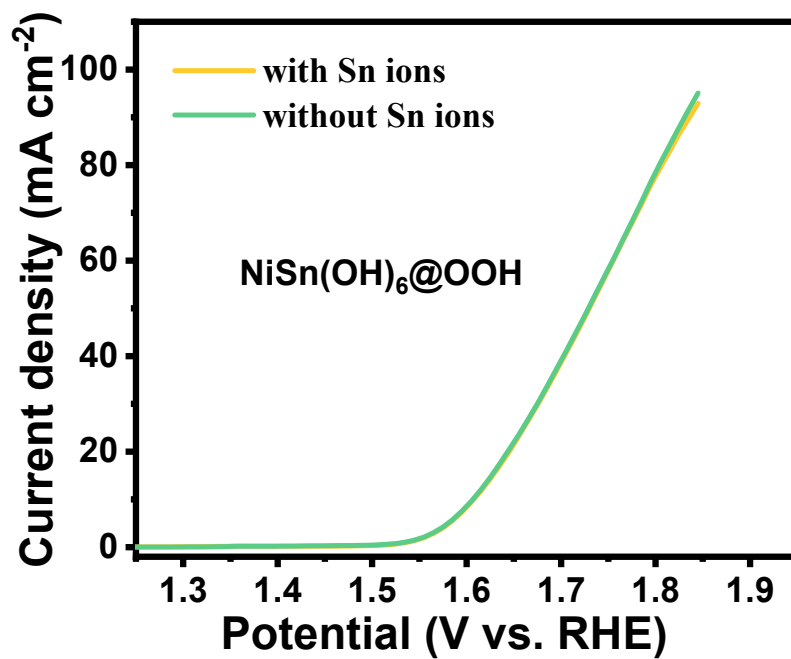
stability test.

Figure S21. LSV curves of the NiSn(OH)$_6$@OOH without iR correction in 1M KOH solution with the presence of Sn ions vs. that in fresh 1M KOH (99.99%) solution without the presence of Sn ions.
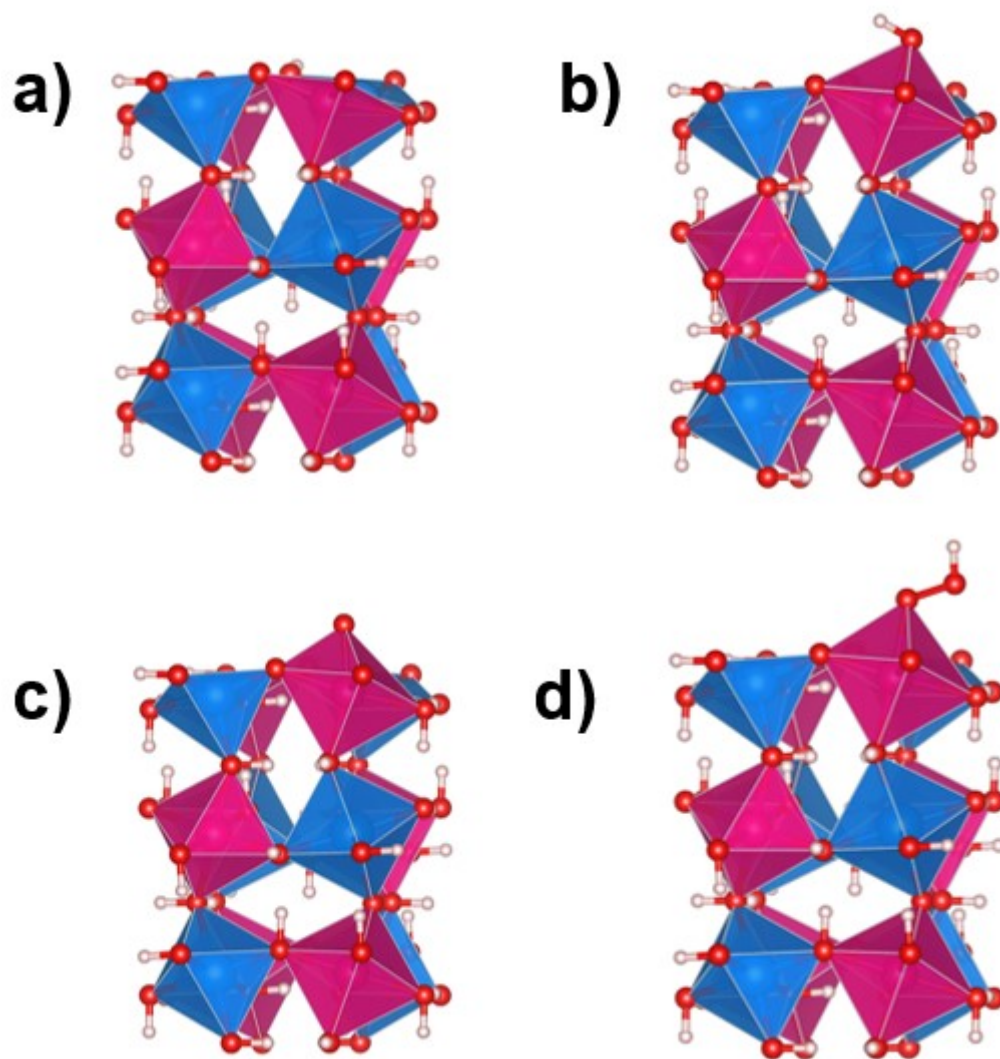
Figure S22. Geometric structures of (a) $NiSn(OH)_6$ and absobed intermediates of (b)

OH*, (c) O*, and (d) OOH* on $NiSn(OH)_6$.
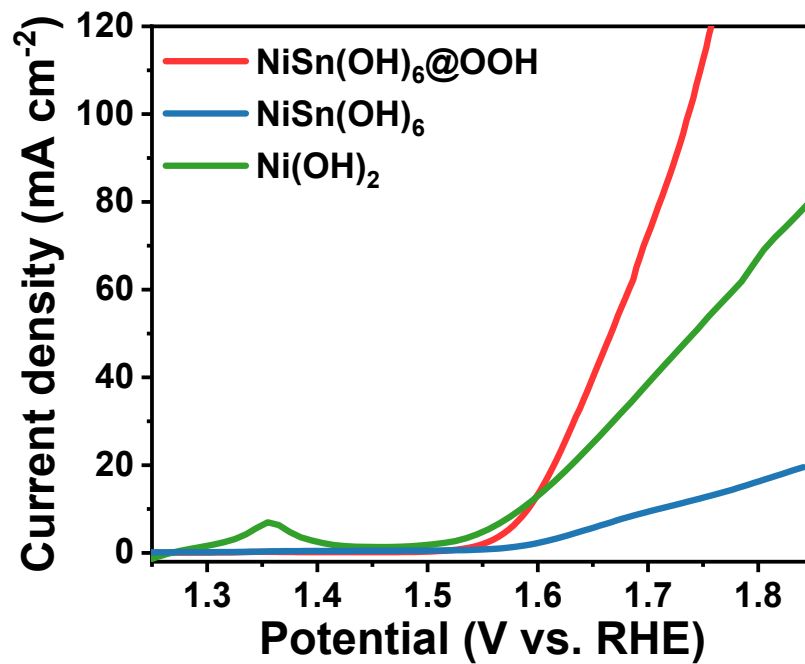
Figure S23. LSV curves of NiSn(OH)$_6$、NiSn(OH)$_6$@OOH and Ni(OH)$_2$ without iR

correction.

Table S1. ICP results of $NiSn(OH)_6$, $SnNiSn(OH)_6@OOH$ and the electrolyte after the CV activation process.

Sample	ICP		
	Sn (ppm)	Ni (ppm)	Atom ration Sn:Ni
$NiSn(OH)_6$	9.687	4.921	0.97
$NiSn(OH)_6@OOH$	7.076	3.973	0.88
Fresh electrolyte	-	-	-
Electrolyte after activation	0.26	-	-

"-" represents below detection limit.

Table S2 Comparison of the OER performance for the Ni-based perovskite materials

Catalysts	$\eta_{@10\ mA\ cm^{-2}}$ (mV)	Loading (mg cm^{-2})	Tafel slop (mV dec^{-1})	References
NiSn(OH)$_6$@OOH	370	0.28	58	This work
b-SnNiFe+Graphene	450	0.25	59	Nat. Commun., 2017, 8, 934
Sr$_{0.95}$Nb$_{0.1}$Co$_{0.9-x}$Ni$_x$O$_{3-\delta}$	438	1	64	J. Mater. Chem. A, 2019, 7, 19453
Ni-exsolved CaTiO$_3$	470	0.06	-	Adv. Energy Mater., 2020, 10, 1903693
LaNiO$_3$	446	0.25	98	Appl. Catal. B: Environ., 2020, 262, 118291
LaNiO$_3$@FeOOH	264	0.25	66	
La$_n$SrNi$_n$O$_{3n+1}$	380	0.10	74	Nano Lett., 2020, 20, 2837
PrNi$_x$Co$_{1-x}$O$_{3-\delta}$-graphene	380	0.30	-	J. Power Sources, 2020, 46, 227234
La$_{n+1}$Ni$_n$O$_{3n+1}$	370	0.07	35	Chem. Eng. J., 2021, 409, 128226
LaMn$_x$Ni$_y$Co$_z$O$_3$	370	0.41	80	J. Energy Chem., 2021, 54, 217
LaNiO$_3$	442	0.10	-	ACS Catal., 2021, 11, 985
La(CrMnFeCo$_2$Ni)O$_3$	325	1.2	51	Adv. Funct. Mater., 2021, 31, 2101632
LaNi$_X$Fe$_{1-X}$O$_{3-\delta}$-QDs/ CNTs	340	0.42	74	Eur. J. Inorg. Chem., 2021, 2225